Jordan Journal of Civil Engineering, Volume **7**, No. **2**, **2013**

Effect of Interfacial Properties on the Behaviour of Retrofitted Members

Yasmeen Taleb Obaidat

Assistant Professor, Department of Civil Engineering, Hijjawi College of Engineering and Technology, Yarmouk University, Irbid 21163, Jordan. E-Mail: yasmin.o@yu.edu.jo

ABSTRACT

Few contributions are available concerning the effect of interfacial properties on the behaviour of retrofitted beams using fibre reinforced polymers. In this paper, finite element analyses of the test specimens from literature were carried out to investigate the effect of interfacial parameters such as, fracture energy, local shear stress and interfacial stiffness on the retrofitted beam performance. Results from the analyses reveal that the load-carrying capacity is significantly influenced by interfacial parameters, fracture energy, local shear stress and interfacial stiffness. Higher shear stress and fracture energy increase the composite action by increasing the maximum load and delaying debonding. The stiffness of the FRP-concrete interface was found to influence the load-carrying capacity and axial strain in FRP. The axial strain in FRP increases by increasing the stiffness of the FRP-concrete interface.

KEYWORDS: Fibre Reinforced Polymer (FRP), Strengthening, Interfacial stiffness, Cohesive model, Fracture energy, Finite Element (FE).

INTRODUCTION

The interface between the Fibre Reinforced Polymer (FRP) and concrete plays a significant role in keeping integrity of the FRP-concrete system. Debonding is the critical problem associated with retrofitted structure using FRP and it prevents the full utilizing of FRP. Debonding occurs due to stress concentration at different places.

Several types of failure modes have been observed in retrofitted RC structures. Concrete failure modes include compression failure before or after steel yielding and shear failure due to shear cracks that extend from the vicinity of the support. FRP rupture failure can also occur before and after steel yielding. The last failure type is debonding of the FRP plate due to stress concentration at the end of the FRP plate or at the bottom of a flexural or shear/flexural crack in the concrete member (Esfahani et al., 2007; Ashour et al., 2004).

A large number of bond tests for the FRP sheet-concrete interfaces under shear have been carried out in the past decades. Test methods include single lap pullout test method (Chajes et al., 1996), double lap pullout bond tests (Sato et al., 2001) and bending tests (Lorenzis et al., 2001).

A local bond–slip model is appropriate to measure bond performance. A local bond–slip relationship is independent of geometric conditions. A great deal of research has been carried out on bond–slip relationships of FRP plate bonded to concrete (Focacci et al., 2000; Nakaba et al., 2001; Yuan et al., 2004; Lu et al., 2005; Pham and Al-Mahaidi, 2007). However, the issues on how to improve the interfacial load transfer performance should have more concern. Still the information on how interfacial properties affect the strengthening capacity is not completely understood. To help overcome this drawback, this study looks into

Accepted for Publication on 19/12/2012.

clarifying the interfacial properties effect on FRR-strengthened structural element using finite element model (FEM). Numerical modelling using the finite element method is a very powerful tool for performing parametric studies in order to improve understanding of physical phenomena, like, for example, debonding in FRP reinforced concrete structures.

DESCRIPTION OF SPECIMENS

Experimental data was obtained from a previous research project (Yao et al., 2005; Woo and Lee, 2010) and from a literature review (Mazzotti et al., 2008). A total of six prisms, strengthened with FRP, were selected for comparison with the numerical results.

Series A corresponds to prisms tested by Yao et al. (2005). The experimental program involved 72 specimens with a total length of 350 mm to investigate the effects of the above-mentioned factors on the bond strength. Two of these specimens were used in this study. Taken into consideration are the length of FRP and the height of concrete free edge. Concrete prisms used were 150 mm wide and of 150 mm total depth. The thickness of FRP was 0.165 mm. The average concrete strength was 23 MPa. The tensile strength and modulus of elasticity of the FRP plates were 4,114 MPa and 256 GPa, respectively. Series B corresponds to prisms tested by Woo and Lee (2010). They studied the effect of FRP-plate length on the bond strength. Their study involved four specimens with a total length of 200 mm. The average compressive strength obtained was 30 MPa. Unidirectional FRP plates with 1.4 mm thickness were used in this investigation. The manufacturer reported an ultimate tensile strength of 2,850 MPa and an elastic modulus of 152.2 GPa. Series C corresponds to prisms tested by Mazzotti et al. (2008). The cross-section of each specimen was of 150 mm width, 200 mm depth, and it was 600 mm long. The compressive strength of concrete was 52.6. FRP plates were used with 50 mm width and 1.2 mm thickness. The modulus of elasticity of the FRP plates was 195.2 GPa. Material properties are presented in Table 2. Details of the testing program can be found in (Yao e al., 2005; Woo and Lee, 2010; Mazzotti et al., 2008).

The fibre reinforcement was applied to one side of the prism. The bonded length of fibre reinforcement on each side is shown in Table 1, for each experimental work. The reinforcement was made by a single layer of FRP plate. The prism was connected to the machine through a steel frame. Strain gauges were mounted on the fibre reinforcement on the bonded length. Geometric properties and mechanical properties of these specimens are shown in Figure 1, Table 1 and Table 2.

MODEL DESCRIPTION

Finite element analysis was performed to model the non-linear behaviour of the prism retrofitted with FRP-plate. The FEM-package ABAQUS/standard 2000 was used for the analysis.

Concrete

The damage plasticity concrete model in ABAQUS/Standard 2000 assumes that the main two failure mechanisms are tensile cracking and compressive crushing. Under uniaxial tension, the stress-strain response follows a linear elastic relationship until the value of the failure stress, f_t, is reached. The failure stress corresponds to the onset of micro-cracking in the concrete material. Beyond the failure stress, the formation of microcracks is represented macroscopically with a softening stress-strain response. Some experimental parameters are not always available in the literature, alternative procedures are required. The concrete tensile strength, f_t, and elastic modulus were estimated from Eq. (1) and Eq. (2) (ACI, 2008), while the concrete fracture energy, G_f (N/m), was estimated using Eq. (3) (Beton, 1993), where $\hat{f}_c$ (MPa) is the concrete compressive strength. Once these parameters (f_t, G_f) have been determined, softening behaviour was modelled using Hillerborg (1985) bilinear curve between the tensile strength and

crack width. Then, the crack opening is calculated from the fracture energy. The tensile damage is specified by an assumed linear relationship between the tension damage variable d_t and the crack opening δ.

$$f_t = 0.35\sqrt{f_c} \quad (1)$$

$$E_c = 4700\sqrt{f_c} \quad (2)$$

$$G_f = G_{fo}\left(\frac{f_c'}{10}\right)^{0.7} \quad (3)$$

where G_{fo} is a constant value related to maximum aggregate size $d_{max.}$

Table 1. Geometric properties of the specimens

Series of Specimens	Width of concrete (mm)	Thickness of concrete (mm)	Length of concrete (mm)	Concrete free edge (h_c) (mm)	Width of FRP (mm)	Thickness of FRP (mm)	Length of FRP (mm)	Max. load (kN)
Series A								
A1	150	150	350	5	25	0.165	75	5.76
A2	150	150	350	120	25	0.165	190	6.02
Series B								
B1	200	200	500	140	50	1.4	250	26
Series C								
C1	150	200	600	-	50	1.2	100	22.3
C2	150	200	600	-	50	1.2	200	19.8
C3	150	200	600	-	50	1.2	400	23

Table 2. Mechanical properties of materials used

		Series A	Series B	Series C
Concrete	f_c (MPa)	23	30	52.6
	f_t (MPa)	-	-	3.81
	E_c (GPa)	-	-	30.7
FRP	E_f (GPa)	256	152.2	195.2
	G_f	1.61	1.2	-
	f_f (GPa)	4.114	2.85	-

Under uni-axial compression, the response is linear until the value of initial yield. In the plastic regime, the response is typically characterized by stress hardening followed by strain softening beyond the ultimate stress. The stress–strain relationship proposed by Saenz (1964) was used to construct the uniaxial compressive stress–strain curve for concrete.

The degradation of the elastic stiffness is characterized by two damage variables, compressive damage variable, d_c, and tensile damage variable, d_t, assumed to be functions of the plastic strains, temperature and field variables. The damage variables can take values from zero, representing the undamaged material, to one, which represents the total loss of strength.

FRP Material

The behaviour of FRP plates is assumed to be linear elastic isotropic until failure. The elastic modulus in the fibre direction of the unidirectional FRP material used in the numerical study was as the value in experimental works in literature, see Table 2.

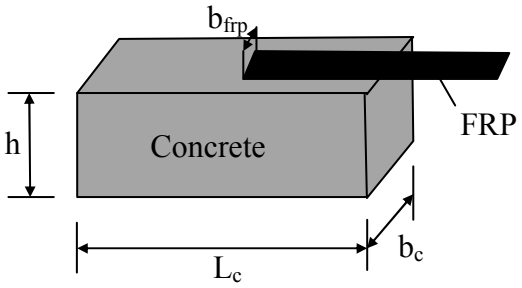

(a)Yao et al. (2005) and Woo and Lee (2010)

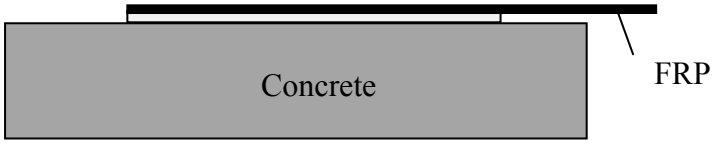

(b)Mazzotti et al. (2008)

Figure 1: Test setup

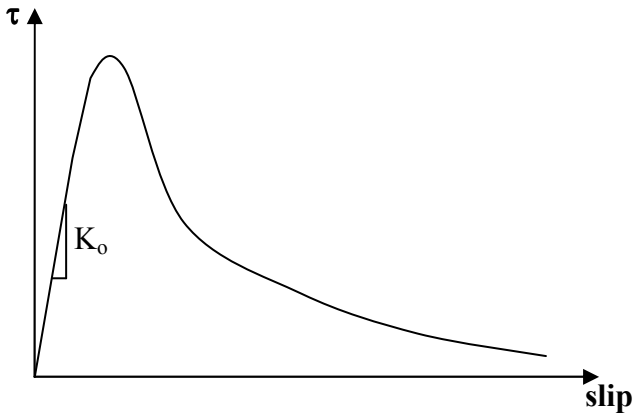

Figure 2: Bond-slip relationship

FRP – Concrete Interface

When debonding failures occur, they usually result from a shear failure of a thin layer of concrete adjacent to the adhesive. In order to represent this failure, an appropriate mesh size was used to capture this performance.

The interface was modelled using a cohesive zone model. The exponential bond slip model (Lu et al., 2005) was used. Figure 2 shows a graphic interpretation of traction-separation law written in terms of the effective traction τ and effective opening displacement δ. The initial stiffness K_o is defined as (Lu et al., 2005):

$$K_o = \frac{1}{\frac{t_i}{G_i} + \frac{t_c}{G_c}} \quad (4)$$

where t_i is the adhesive thickness, t_c is the concrete thickness and G_i and G_c are the shear modulus of adhesive and concrete, respectively.

The maximum shear stress, τ_{max}, was obtained from Eq. (5) (Lu et al., 2005). On the other hand, the value of fracture energy is not determined in the experimental work. Eq. (6) (Lu et al., 2005) was used to determine this value for the numerical purpose.

$$\tau_{max} = 1.5\,\beta_w f_{ct} \quad (5)$$

$$G_f = 0.308\beta_w^{\,2}\sqrt{f_{ct}} \quad (6)$$

where;

$$\beta_w = \sqrt{\left(2.25 - {}^{b_f}/_{b_c}\right)/\left(1.25 + {}^{b_f}/_{b_c}\right)}$$

NUMERICAL ANALYSIS

The four-node quadratic elements were used for the concrete and FRP. The eight-node 3-D cohesive elements were used to model the interface layer. The cohesive interface elements are composed of two surfaces separated by a thickness. The relative motion of the bottom and top parts of the cohesive element measured along the thickness direction represents an opening or closing of the interface. The relative motion of these parts represents the transverse shear behaviour of the cohesive element.

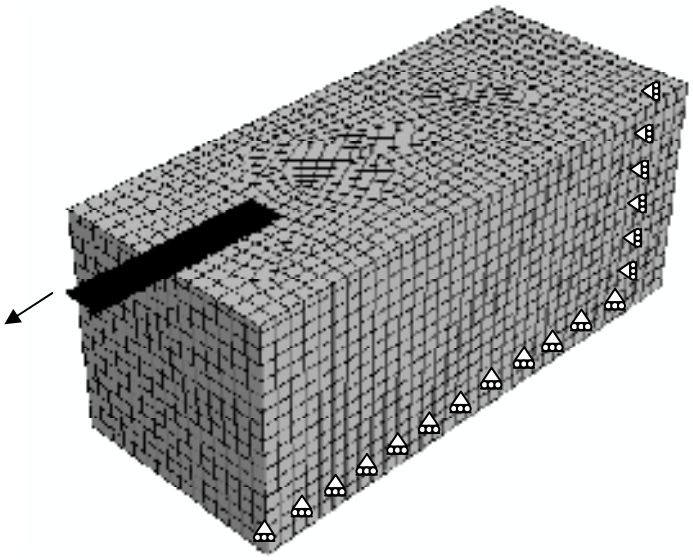

Figure 3: Finite element mesh of specimens

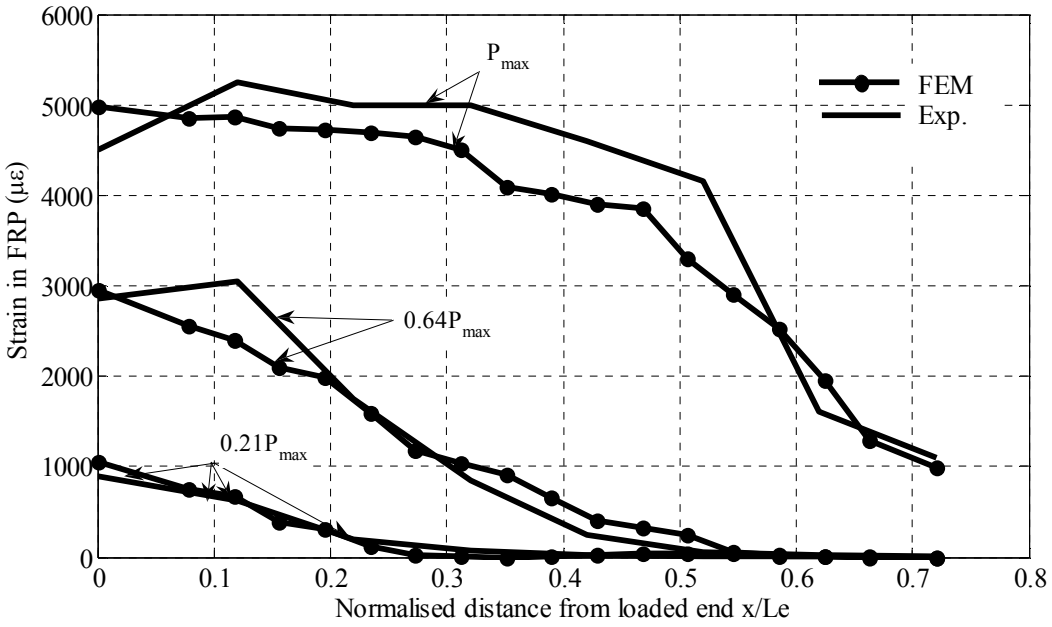

(a) Series A-A1.

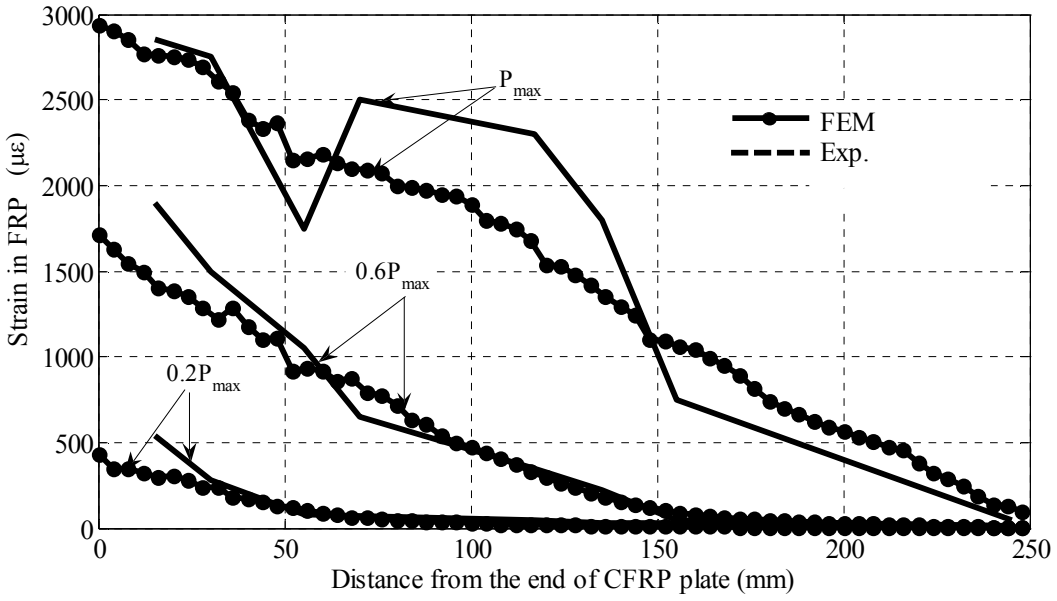

(b) Series B.

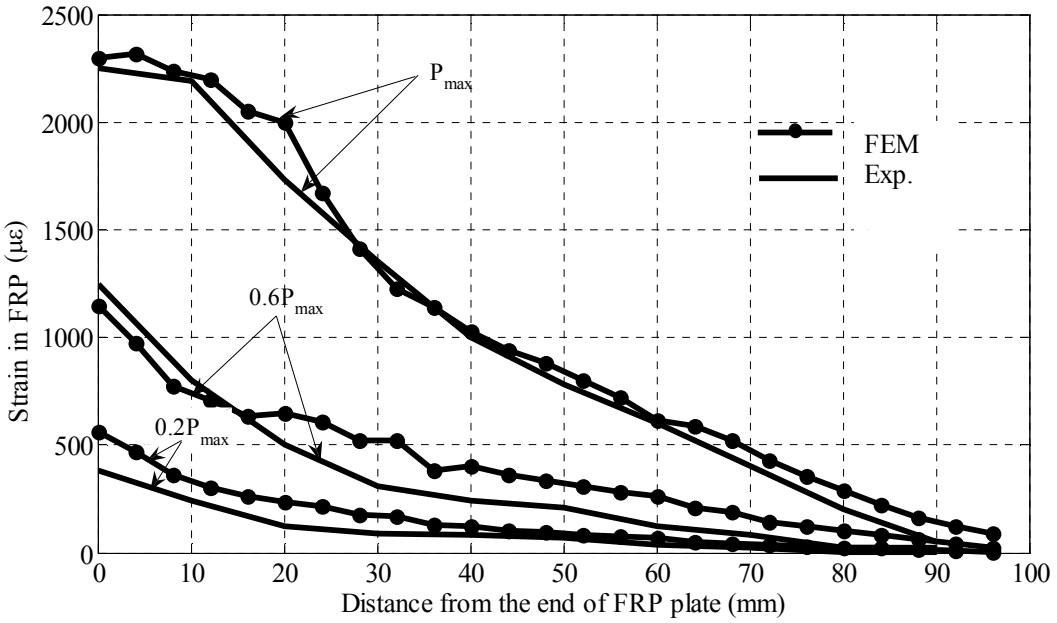

(c) Series C-C1.

Figure 4: FRP reinforcement strain distribution for the shape of bond-slip

In this study, the total deflection applied was divided into a series of deflection increments. Newton method iterations provide convergence, within tolerance limits, at the end of each deflection increment. During concrete cracking and the ultimate stage where a large number of cracks occur, the deflections are applied with gradually smaller increments. Automatic stabilization and small increment time were also used to avoid diverged solution. In addition, an appropriate mesh size was used, see Figure 3.

RESULTS

Comparison between FEM and Experimental Work

The finite element results were compared with the test results from the literature review (Yao et al., 2005; Woo and Lee, 2010; Mazzotti et al., 2008). One specimen was chosen to represent the result from each paper as shown in Figure 4.

From the analysis results obtained by each model, there is small difference in maximum tensile force among the model and experimental work. The strain results were compared in three different load levels 0.2, 0.6 and 1 of maximum loading level mentioned in Table 1, see Figure 3. It is shown that for all specimens, the finite element strain results are almost the same for model and experimental results. For the load levels under 0.2 of maximum load, before debonding occurs, there is almost no difference between the results from the model and experimental works. For the maximum load, there is a deviation compared to the test results of specimens from Yao et al. (2005), A1, Woo and Lee (2010), B1, and Mazzotti et al. (2008), C1, but the finite element strain results still compare well with test results. This means that after debonding, the difference exists due to the random appearance of local debonding. Nevertheless, it seems that the strain results obtained from models compare well with the test results especially in the lower load levels.

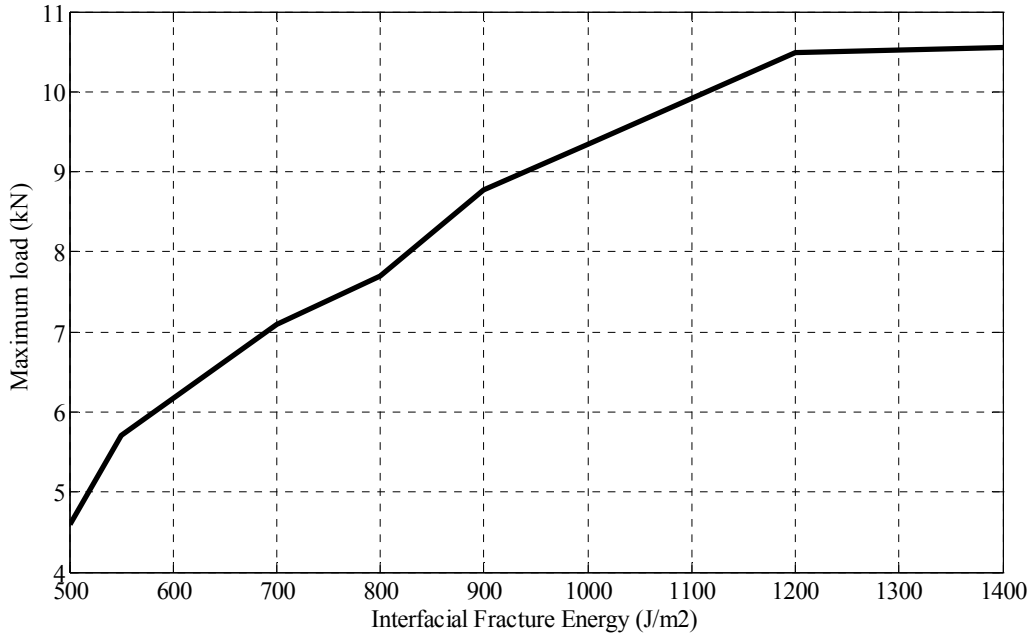

(a) Series A-A2, where Le=105 mm

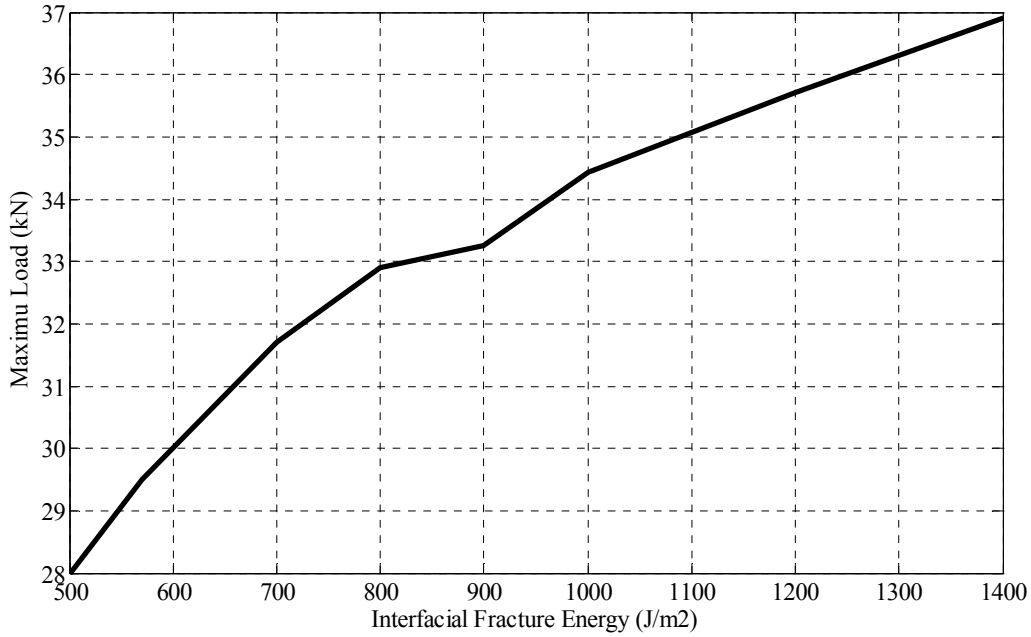

(b) Series B.

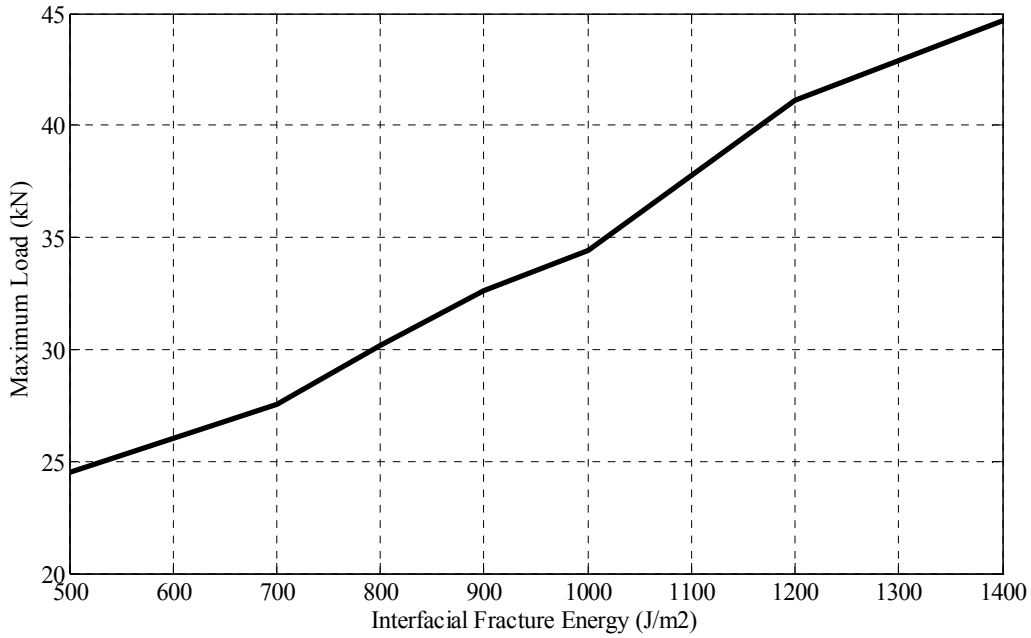

(c) Series C-C2

Figure 5: Maximum load for various interfacial fracture energies

Interfacial Fracture Energy

This study focuses on how fracture energy affects strengthening behaviour. By fixing shear stress as calculated from Eq. (5), the effect of interfacial fracture energy is studied by varying it.

Figure 5 shows the maximum load *versus* the fracture energy. The figure clearly shows that the maximum load increases with interfacial fracture energy. This can be attributed to the fact that large interfacial fracture energy yields to delay debonding, and thus more external work is required to create the interfacial debonding.

Figure 6 illustrates the FRP strain distribution along the interface for all energy values at maximum load. The figure shows that higher interfacial fracture energy interfaces increase the utilizing of full potential of the strengthening system. It can be seen that the strain of the FRP increases noticeably with increasing the interfacial energy. This is attributed to the macro-debodning that exists when employing low energy interfaces, and then the FRP plate debonds before it can maximize its strengthening potential. Therefore, higher energy interfaces are able to increase the utilizing of FRP in the strengthening system since the onset of debonding is delayed.

Shear Stress

The interfacial shear stress between the FRP and concrete plays a significant role in the bond between FRP and concrete. Therefore, the present study considered the interfacial shear stress. By fixing the initial interfacial stiffness and the interfacial fracture energy as calculated in previous studies available in the literature, the effect of local shear stress is studied by varying it: τ = 1, 3, 5, 7, 9 and 11MPa.

As shown in Figure 7, a higher value of shear stress model provides a higher load than the other lower value of shear stress model. This may be attributed to the higher value of shear stress model being capable of delaying the initiation of debonding.

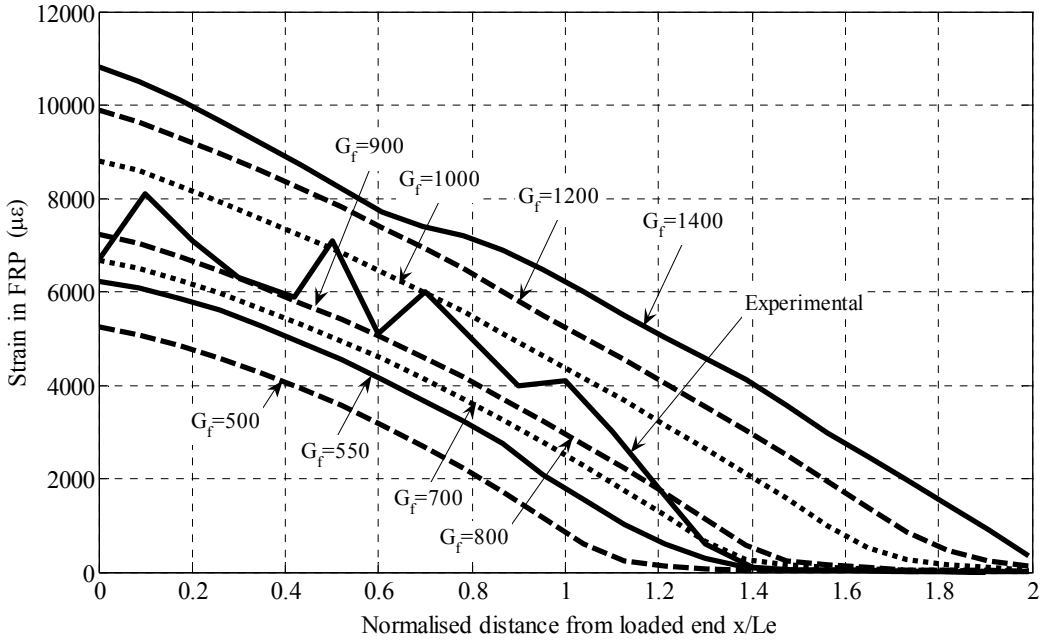

(a) Series A-A2, where Le=105 mm

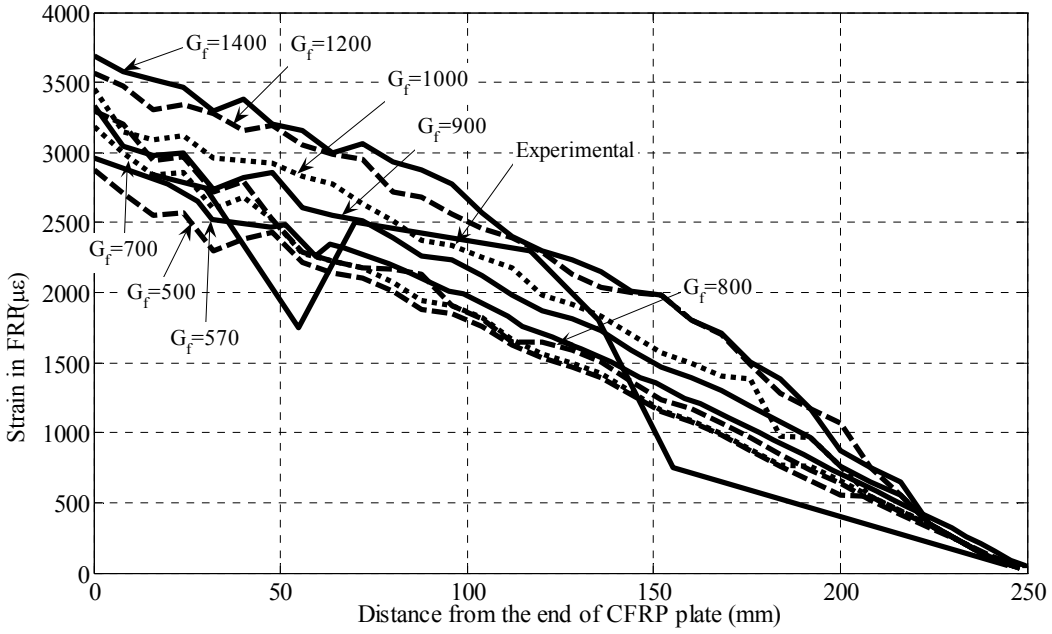

(b) Series B

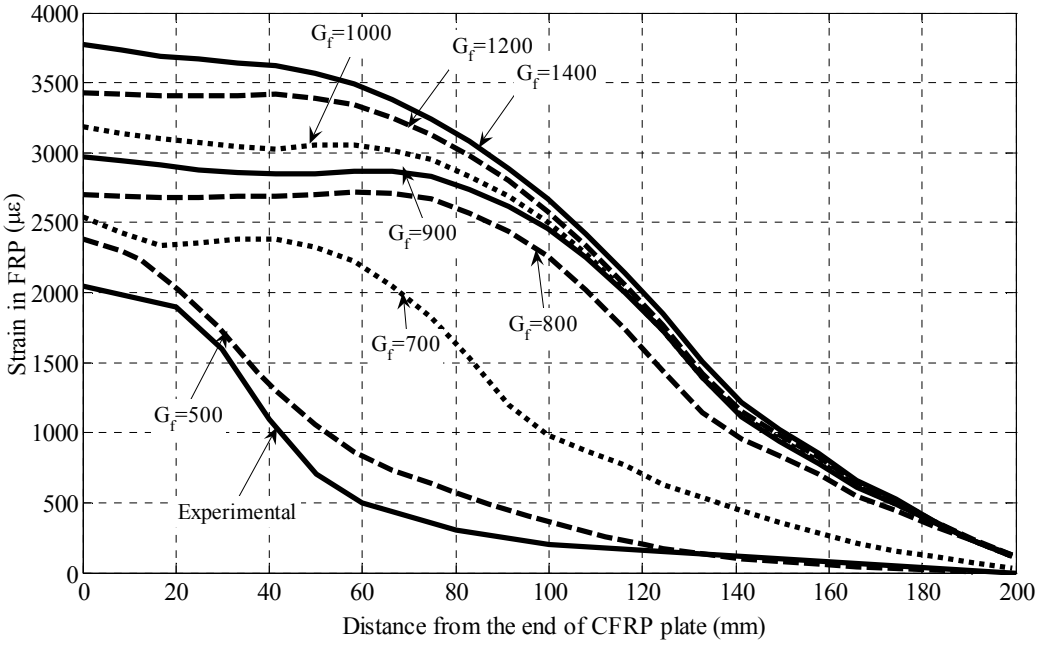

(c) Series C-C2

Figure 6: FRP strain distribution at maximum load for various interfacial fracture energies

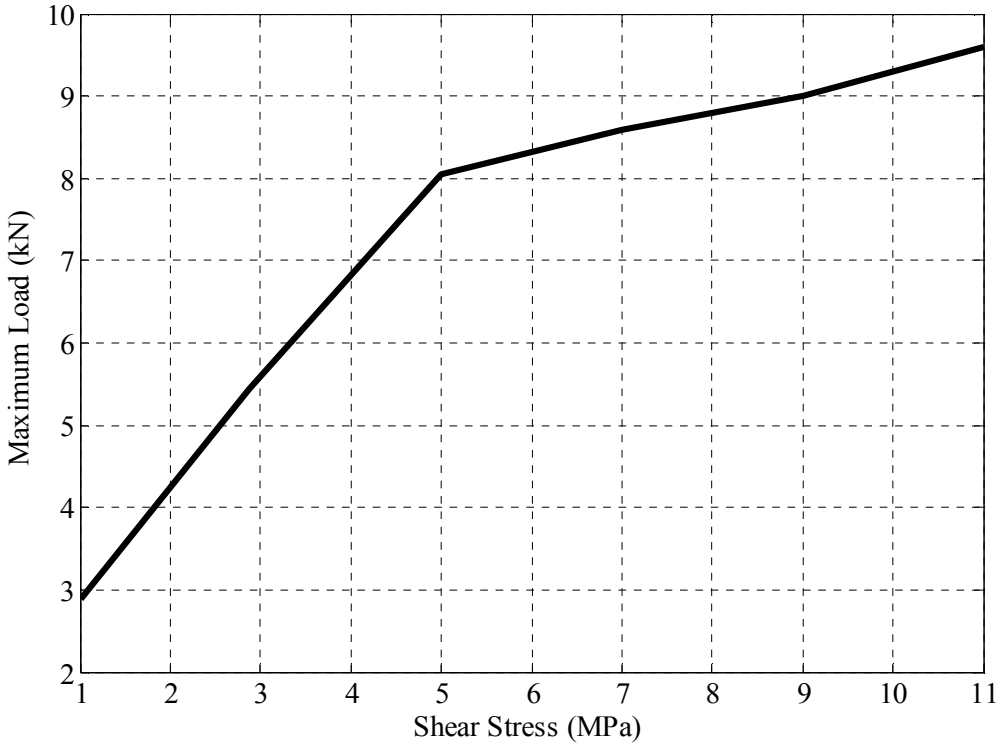

(a) Series A-A1

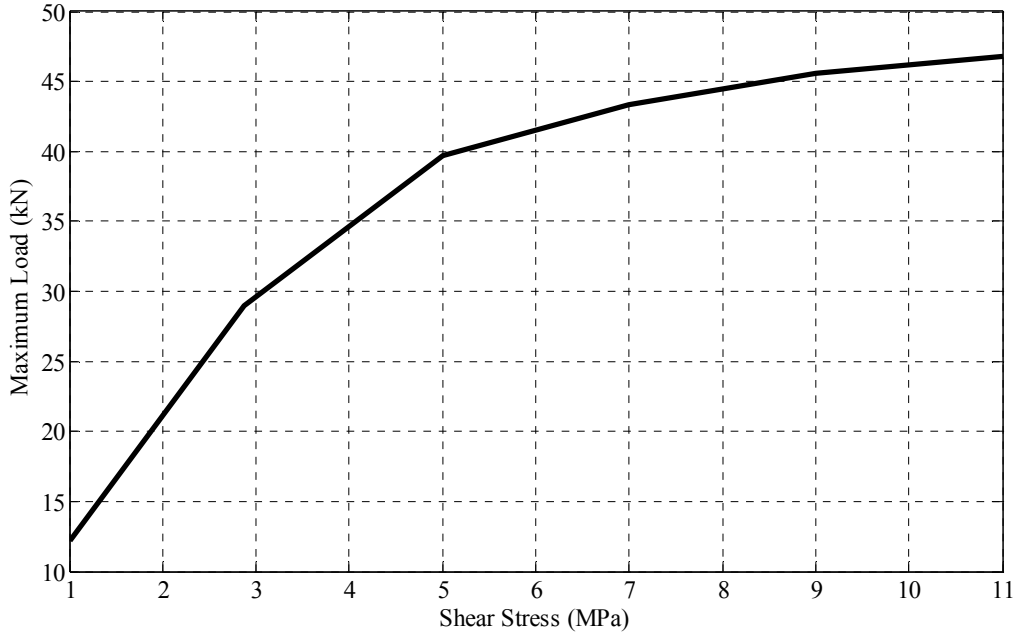

(b) Series B

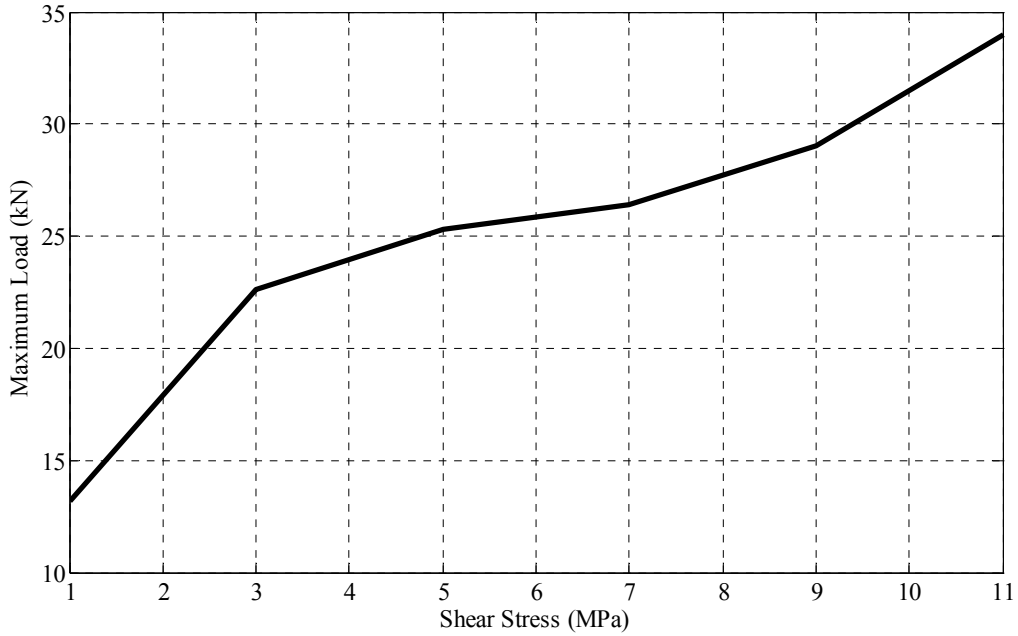

(c) Series C-C3

Figure 7: Maximum load for various shear stresses

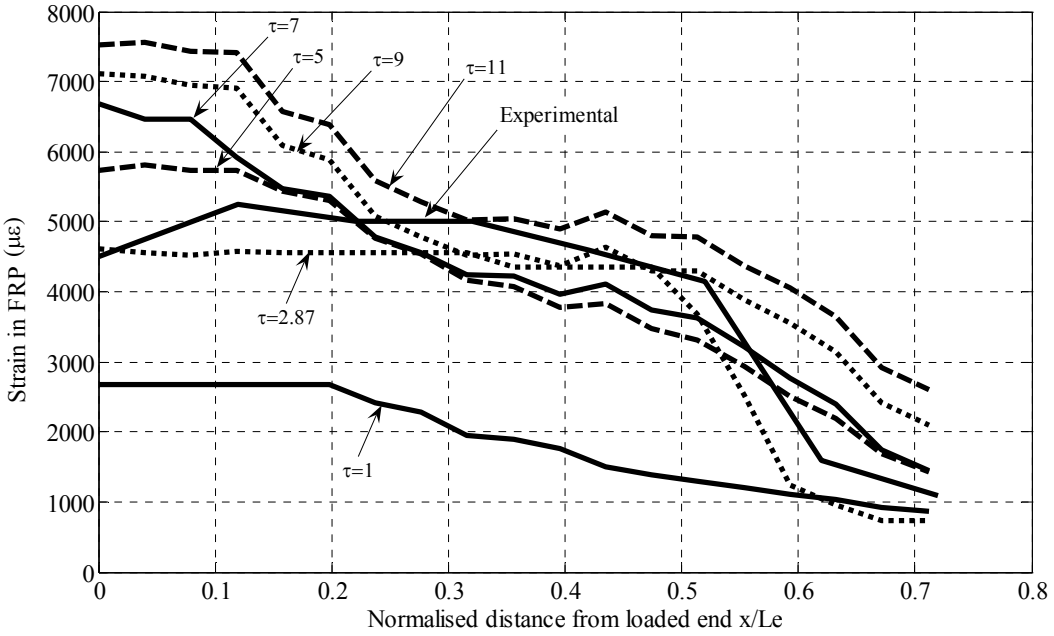

(a) Series A-A1

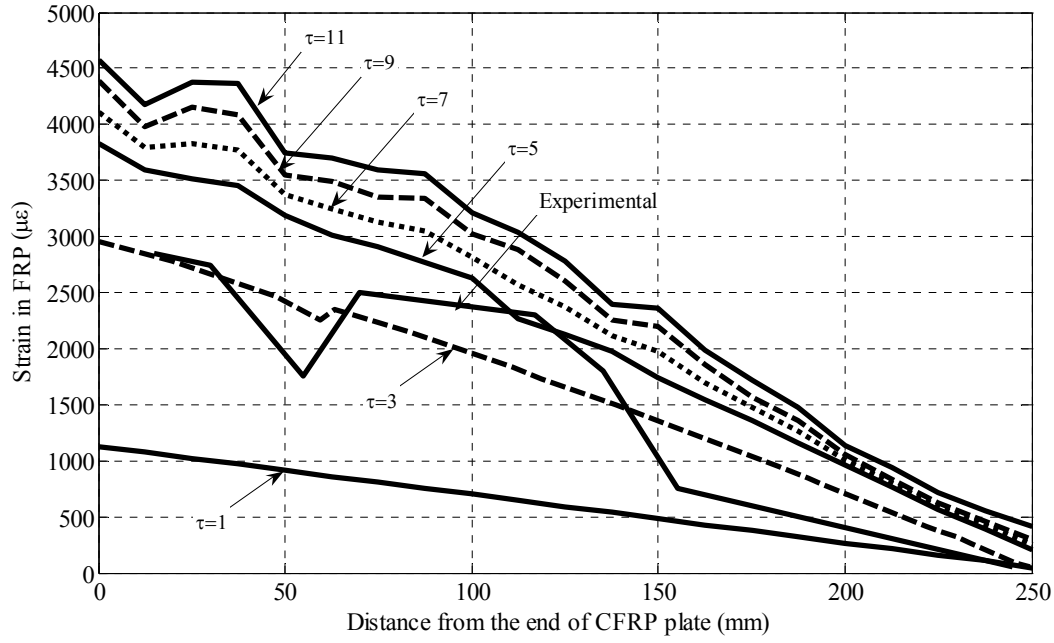

(b) Series B

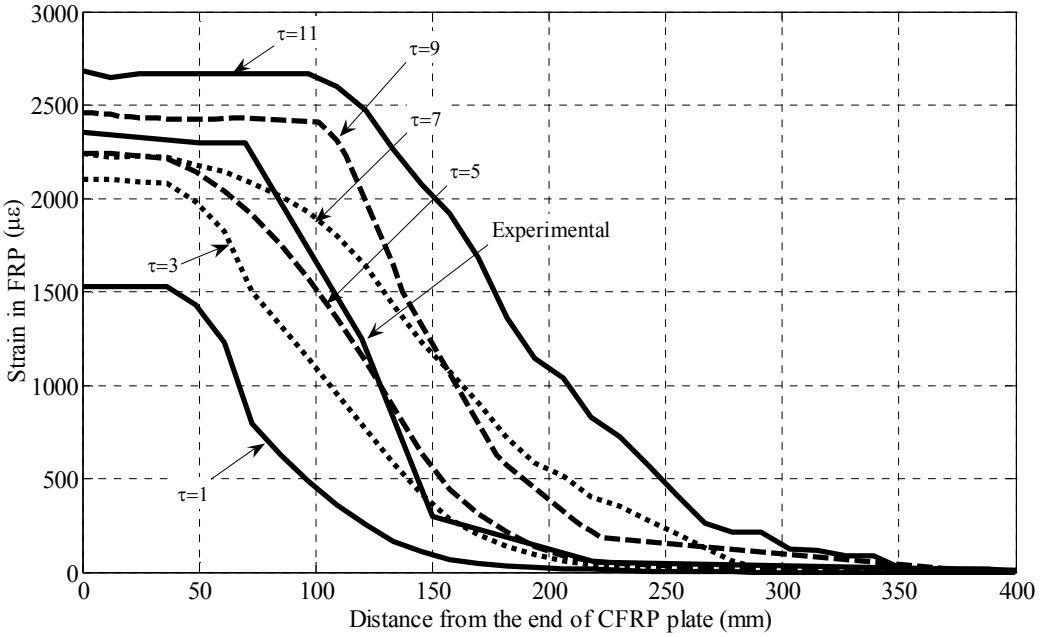

(c) Series C-C3

Figure 8: FRP strain distribution at maximum load for various shear stresses

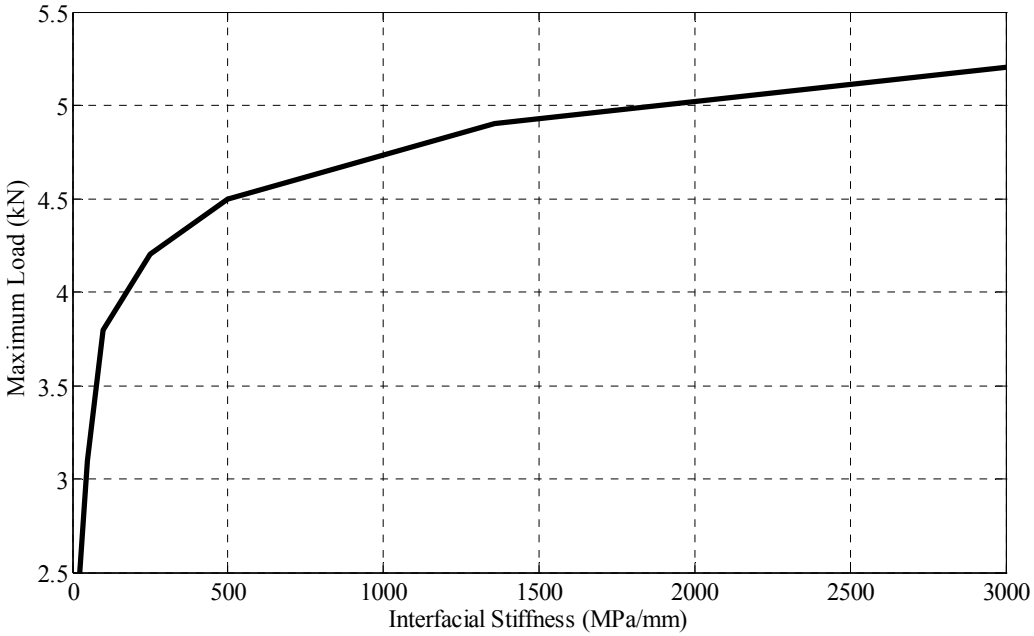

(a) Series A-A1

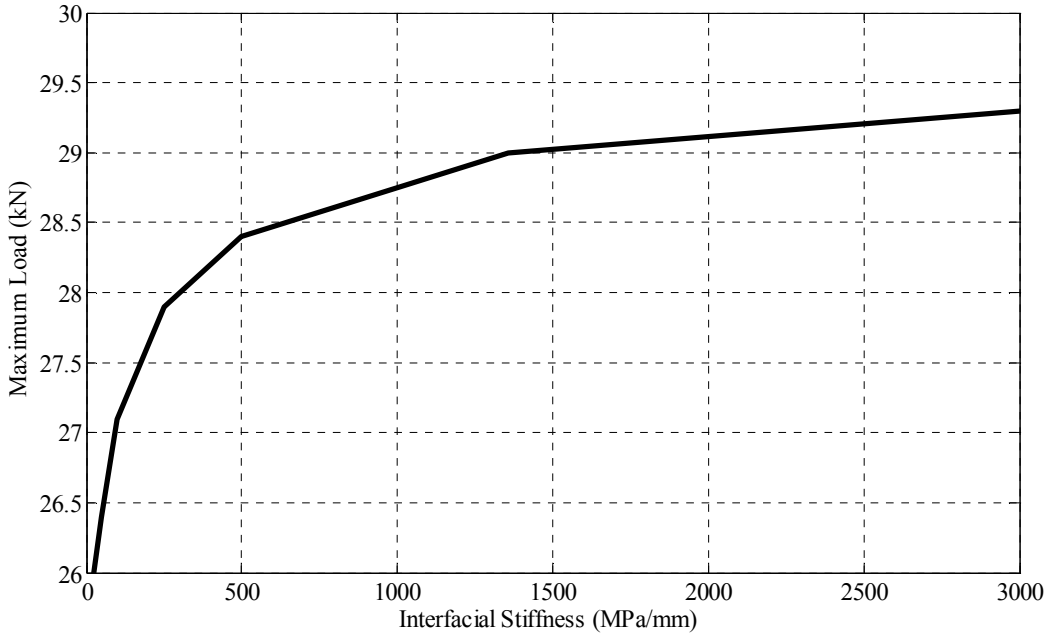

(b) Series B-B1

Figure 9: Maximum load for various values of interfacial stiffness

Figure 8 illustrates the FRP strain development along the interface for the different shear stress models at maximum load. The findings show that the higher value of shear stress increase the rate of stress transfer along the interface (strain increase) and utilize the FRP material to a higher extent. The strain in the FRP plate of the 11MPa model is found to be greater than the other shear stress bond values. This may be attributed to the higher value of shear stress model being capable of delaying the initiation of debonding and thereby transferring more stress to the FRP plate.

Interfacial Stiffness

Interfacial stiffness is directly related to the properties of the adhesive, shear modulus and thickness of the adhesive in contact with the concrete and the initial layer of the concrete substrate. It has a direct influence on the load transfer efficiency between the concrete substrate and the FRP. For this reason, an effort was made to investigate its effect on strengthening. By fixing local shear stress and interfacial fracture energy, the effect of interfacial stiffness is studied by varying it: K_o= 25, 50, 100, 250, 500, 1500 and 3000 MPa/mm.

Figure 9 shows the maximum load *versus* interfacial stiffness. It can be seen that higher interfacial stiffness results in a higher load than lower stiffness. This is due to the fact that a low value of interfacial stiffness results in a slow stress transfer in comparison to higher stiffness. This enforces the concrete to carry a higher load level resulting in earlier formation of cracking, which leads to the initiation of debonding.

As shown in Figure 10, a low value of interfacial stiffness results in low strain distribution. In other words, a low value of interfacial stiffness results in a low rate of stress transfer to the concrete (low stain in FRP). This leads to earlier formation of cracking in concrete and initiation of debonding.

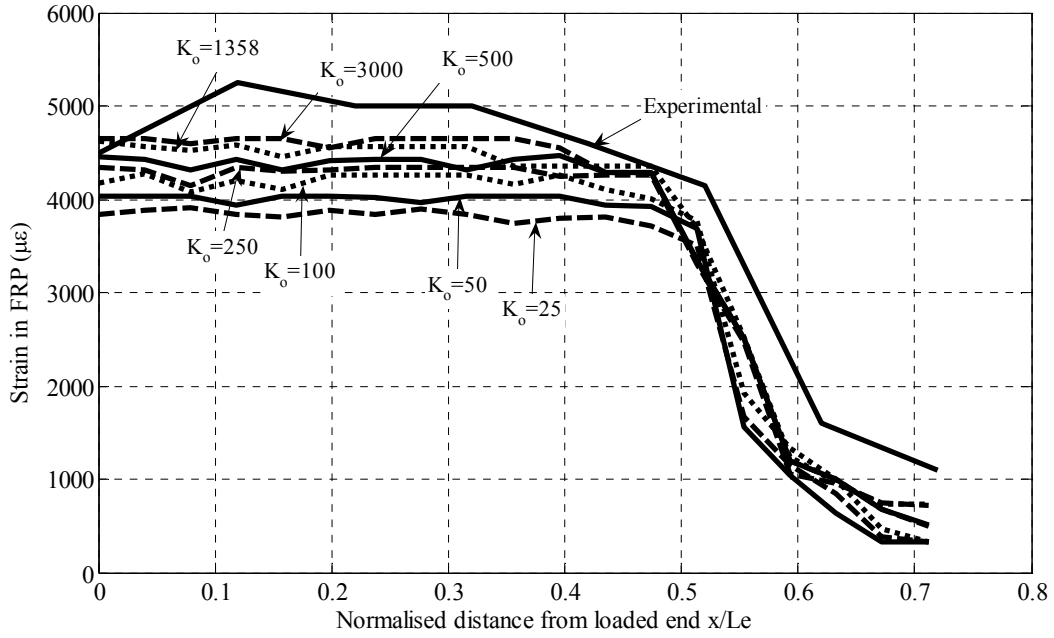

(a) Series A-A1

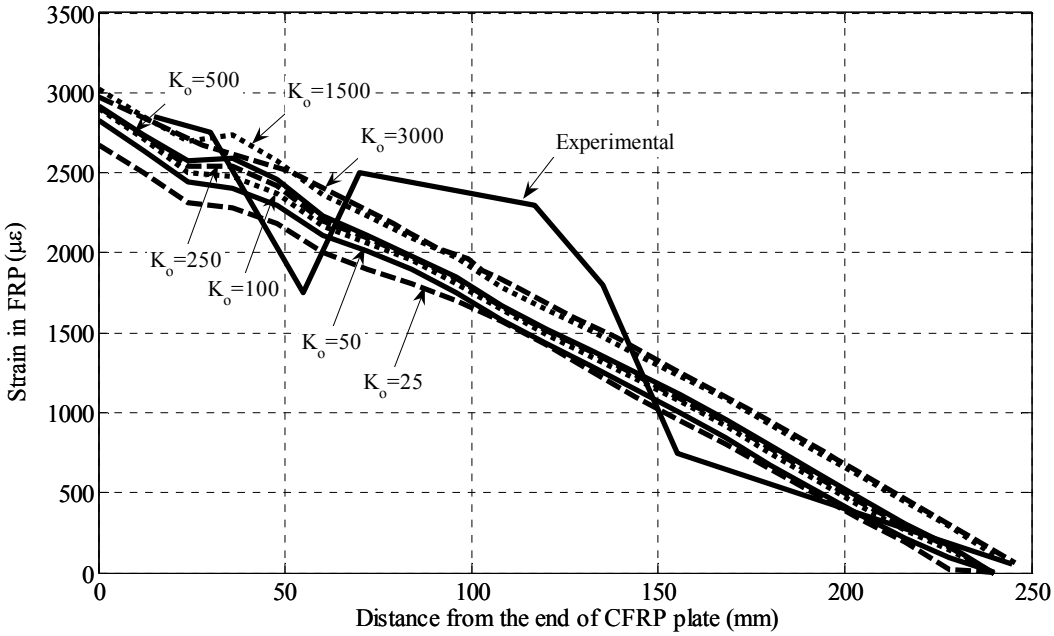

(b) Series B-B1

Figure 10: FRP strain distribution at maximum load for various values of interfacial stiffness

CONCLUSIONS

A finite element model accounting for material non-linearity has been developed and successfully verified against experimental work. A parametric study has been performed to study the effects of interfacial properties, fracture energy, local shear stress and interfacial stiffness. The following conclusions are drawn:

- An increase in fracture energy always gives an increase in FRP utilization. The maximum load of strengthened prism increases with interfacial fracture energy.
- Maximum load increases with increasing local shear stress. In addition, axial strain in FRP increases with increasing this parameter.
- A high value of interfacial stiffness will give a maximum load. One reason for this is that a low value of interfacial stiffness results in a slow stress transfer in comparison to higher stiffness, where otherwise a larger part of the axial load will be carried by the concrete, which means that cracks will develop in concrete, which leads to the initiation of debonding.

REFERENCES

ACI Committee 318. 2008. Building code requirements for structural concrete and commentary (ACI 318-2008). American Concrete Institute, Detroit, MI.

Ashour, A.F., El-Refaie, S.A. and Garrity, S.W. 2004. Flexural strengthening of RC continuous beams using CFRP laminates. *Cement and Concrete Composites*, 26: 765-775.

Beton, C. E.-I. 1993. CEB-FIP model code 1990 (CEB-FIP MC90). *Bulletin D'Information*, 215, Lausanne.

Chajes, M. J., Finch, W. W., Januszka, T. F. and Thomson, T. A. 1996. Bond and force transfer of composite material plates bonded to concrete. *ACI Structures Journal*, 93 (2): 208-217.

Esfahani, M., Kianoush, M. and Tajari, A. 2007. Flexural behaviour of reinforced concrete beams strengthened by CFRP sheets. *Engineering Structures*, 29: 2428-2444.

Focacci, F., Nanni, A. and Bakis, C.E. 2000. Local bond-slip relationship for FRP reinforcement in concrete. *Journal Composite Construction, ASCE*, 4 (1): 24-31.

Hibbitt, Karlsson, Sorensen and Inc. 2000. ABAQUS theory manual, user manual, example manual, Version 6.7. Providence, RI.

Hillerborg, A. 1985. The theoretical basis of a method to determine the fracture energy G_f of concrete. *Materials and Structures, RILEM 50-FMC*, 1985; 108: 291-296.

Lorenzis, L. De., Miller, B. and Nanni, A. 2001. Bond of fibre-reinforced polymer laminates to concrete. *ACI Materials Journal*, 98 (3): 256-264.

Lu, X.Z., Teng, J.G., Ye, L.P. and Jiang, J.J. 2005. Bond-slip models for FRP sheets/plates bonded to concrete. *Eng. Struct.,* 27 (6): 920-937.

Mazzotti, C., Savoia, M. and Ferracuti, B. 2008. An experimental study on delamination of FRP plates bonded to concrete. *Construction and Building Materials*, 22: 1409-1421.

Nakaba, K., Kanakubo, T., Furuta, T. and Yoshizawa, H. 2001. Bond-behaviour between fiber-reinforced polymer laminates and concrete. *ACI Struct. J.*, 98 (3): 359-367.

Pham, H. and Al-Mahaidi, R. 2007. Modelling of CFRP-concrete shear-lap tests. *Construction and Building Materials,* 21 (4): 727-735.

Saenz, L. 1964. Discussion equation for the stress - strain curve of concrete. By Desayi, P. and Krishnan, S. *ACI Journal*, 61:1229-1235.

Sato, Y., Asano, Y. and Ueda, T. 2001. Fundamental study on bond mechanism of carbon fiber sheet. *Concrete Library International*, *JSCE,* 37: 97-115.

Woo, S.K. and Lee, Y. 2010. Experimental study on interfacial behavior of CFRP-bonded concrete. *KSCE Journal of Civil Engineering,* 14 (3):385-393.

Yao, J., Teng, J.G. and Chen, J.F. 2005. Experimental study on FRP-to-concrete bonded joints. *Composites: Part B*, 36: 99-113.

Yuan, H., Teng, J.G., Seracino, R., Wu, Z.S. and Yao, J. 2004. Full-range behaviour of FRP-to concrete bonded joints. *Eng. Struct.,* 26 (5): 553-565.